Contribution from the Department of Chemistry and Materials Research Center, Northwestern University, Evanston, Illinois 60208

Thermally Activated Magnetic Interactions in a One-Dimensional Semiconductor. Structural, Charge-Transport, and Magnetic Studies of $[Cu(tmp)]_2[ReO_4]$

Ellen M. McGhee, Martin R. Godfrey, Brian M. Hoffman,* and James A. Ibers*

Received May 10, 1990

Electrochemical oxidation of (5,10,15,20-tetramethylporphyrinato)copper(II), Cu(tmp), in the presence of the perrhenate ion affords the new molecular conductor $[Cu(tmp)]_2[ReO_4]$. The compound is composed of partially oxidized ($+^1/_2$) Cu(tmp) cations stacked metal-over-metal and surrounded by chains of ReO_4 anions. Single-crystal, room-temperature conductivity along the needle (crystallographic *c*) axis averages 40 Ω^{-1} cm^{-1}, lower than the values previously reported for Ni(tmp)-based conductors. The conductivity is thermally activated and may be fit to an expression that describes a semiconductor with temperature-dependent carrier mobility: $\sigma = \sigma_0 T^{-\alpha} \exp(-\Delta E/k_B T)$ (ΔE = 0.126 (2) eV, α = 3.8 (2)). Magnetic studies show that the local Cu(II) moments and the itinerant π-carrier electrons participate in strong spin exchange. This intramolecular Cu-π coupling is shown to mediate Cu-Cu spin exchange along the linear chains of Cu(II) ions found in this compound. These magnetic interactions depend on the thermally activated carrier concentration. The angular variation of the line width indicates that exchange is highly one-dimensional. The compound crystallizes in space group C^3_{4h}-$P4/n$ of the tetragonal system with two formula units in a cell of dimensions *a* = 16.774 (9) Å and *c* = 6.746 (4) Å (V = 1898 Å^3) at 110 K. Full-matrix least-squares refinement of 144 variables gives a final value of 0.069 for the *R* index on F^2 for 4695 unique observations and a value of 0.043 for the *R* index on *F* for the 2582 observations having $F_o^2 > 3\sigma(F_o^2)$.

Introduction

Partial oxidation of metalloporphyrins yields a variety of electronically conductive solids.[1-12] Many of these exhibit the same basic structural motif: chains of anions surrounding metal-over-metal stacks of metallomacrocycles.[13] One such conductor may be prepared by chemical oxidation of Ni(pc) (pc = phthalocyaninato) with molecular iodine and has the composition Ni(pc)I.[1] The phthalocyaninato ligand is partially ($+^1/_3$) oxidized in this compound, and the iodine is present as linear chains of I_3^- anions. Ni(pc)I is a highly conductive molecular metal ($\sigma_{RT} \approx$ 500 Ω^{-1} cm^{-1}) that retains a metallic band structure to very low temperatures.[1]

A molecular metal isostructural with Ni(pc)I may be prepared by oxidation of Cu(pc) with iodine. In Cu(pc)I the conduction pathway is also through the phthalocyaninato ligands, but carrier electrons in the ligand-based p-π conduction band participate in strong spin exchange with the Cu(II) ions (d^9, $S = {}^1/_2$) at the center of each macrocycle.[2] This intramolecular interaction between localized Cu(II) moments and mobile π-carriers leads to long-range carrier-mediated Cu-Cu coupling along the linear chains of Cu(II) sites and gives rise to interesting magnetic phenomena at low temperatures. Similar behavior is seen in Cu(tatbp)I.[3]

We now report the synthesis and properties of $[Cu(tmp)]_2[ReO_4]$, a ligand-oxidized conductor. Strong intramolecular spin exchange between the localized Cu(II) moments and the electrons in the partially occupied p-π band is again observed in this compound. However, $[Cu(tmp)]_2[ReO_4]$ is semiconducting rather than metallic, and ESR studies indicate that the magnetic properties of this compound depend on the thermally activated carrier concentration and that exchange along a Cu(II) chain is highly one-dimensional, as reported for the related system $[Cu(tatbp)_3][ReO_4]_2 \cdot C_{10}H_7Cl$.[4]

Table I. Crystal Data and Experimental Details for $[Cu(tmp)]_2[ReO_4]$

compd	bis[(5,10,15,20-tetramethylporphyrinato)-copper(II)] perrhenate
formula	$C_{48}H_{40}Cu_2N_8O_4Re$
fw	1106.20
a, Å	16.774 (9)
c, Å	6.746 (4)
V, Å^3	1898
Z	2
temp, K	110[a]
d_{calc}, g/cm^3	1.935
space group	C^3_{4h}-$P4/n$
radiation	Mo Kα (λ(Mo Kα_1) = 0.7093 Å); graphite-monochromated
μ, cm^{-1}	44.0
transm coeff[b]	0.594-0.668
R on F_o^2	0.069
R_w on F_o^2	0.103
R on F_o with $F_o^2 > 3\sigma(F_o^2)$	0.043

[a] The low-temperature system is based on a design by: Huffman, J. C. Ph.D. Thesis, Indiana University, 1974. [b] The analytical absorption correction was performed with the use of the Northwestern absorption program AGNOST. See: de Meulenaer, J.; Tompa, H. *Acta Crystallogr.* **1965**, *19*, 1014-1018.

(1) (a) Schramm, C. J.; Scaringe, R. P.; Stojakovic, D. R.; Hoffman, B. M.; Ibers, J. A.; Marks, T. J. *J. Am. Chem. Soc.* **1980**, *102*, 6702-6713. (b) Martinsen, J.; Greene, R. L.; Palmer, S. M.; Hoffman, B. M.; Ibers, J. A. *J. Am. Chem. Soc.* **1983**, *105*, 677-678. (c) Martinsen, J.; Palmer, S. M.; Tanaka, J.; Greene, R. L.; Hoffman, B. M. *Phys. Rev. B* **1984**, *30*, 6269-6276.

(2) (a) Ogawa, M. Y.; Martinsen, J.; Palmer, S. M.; Stanton, J. L.; Tanaka, J.; Greene, R. L.; Hoffman, B. M.; Ibers, J. A. *J. Am. Chem. Soc.* **1987**, *109*, 1115-1121. (b) Ogawa, M. Y.; Hoffman, B. M.; Lee, S.; Yudkowsky, M.; Halperin, W. P. *Phys. Rev. Lett.* **1986**, *57*, 1177-1180.

(3) Tatbp = triazatetrabenzoporphyrinato dianion. (a) Liou, K. K.; Ogawa, M. Y.; Newcomb, T. P.; Quirion, G.; Lee, M.; Poirier, M.; Halperin, W. P.; Hoffman, B. M.; Ibers, J. A. *Inorg. Chem.* **1989**, *28*, 3889-3896. (b) Quirion, G.; Poirier, M.; Ogawa, M. Y.; Hoffman, B. M. *Solid State Commun.* **1987**, *64*, 613-616. (c) Quirion, G.; Poirier, M.; Liou, K. K.; Ogawa, M. Y.; Hoffman, B. M. *Phys. Rev. B* **1988**, *37*, 4272-4275.

(4) (a) Godfrey, M. R.; Liou, K. K.; Newcomb, T. P.; Halperin, W. P.; Hoffman, B. M.; Ibers, J. A. *Synth. Met.* **1989**, *29*, F51-F58. (b) Godfrey, M. R.; Newcomb, T. P.; Hoffman, B. M.; Ibers, J. A. *J. Am. Chem. Soc.* **1990**, *112*, 7260-7269.

(5) Newcomb, T. P.; Godfrey, M. R.; Hoffman, B. M.; Ibers, J. A. *Inorg. Chem.* **1990**, *29*, 223-228.

(6) Newcomb, T. P.; Godfrey, M. R.; Hoffman, B. M.; Ibers, J. A. *J. Am. Chem. Soc.* **1989**, *111*, 7078-7084.

(7) Martinsen, J.; Stanton, J. L.; Greene, R. L.; Tanaka, J.; Hoffman, B. M.; Ibers, J. A. *J. Am. Chem. Soc.* **1985**, *107*, 6915-6920.

(8) Hoffman, B. M.; Ibers, J. A. *Acc. Chem. Res.* **1983**, *16*, 15-21.

(9) Pace, L. J.; Martinsen, J.; Ulman, A.; Hoffman, B. M.; Ibers, J. A. *J. Am. Chem. Soc.* **1983**, *105*, 2612-2620.

(10) Yakushi, K.; Sakuda, M.; Hamada, I.; Kuroda, H.; Kawamoto, A.; Tanaka, J.; Sugano, T.; Kinoshita, M. *Synth. Met.* **1987**, *19*, 769-774.

(11) (a) Almeida, M.; Kanatzidis, M. G.; Tonge, L. M.; Marks, T. J.; Marcy, H. O.; McCarthy, W. J.; Kannewurf, C. R. *Solid State Commun.* **1987**, *63*, 457-461. (b) Marks, T. J. *Angew. Chem., Int. Ed. Engl.* **1990**, *29*, 857-879.

(12) Yakushi, K.; Yamakado, H.; Yoshitake, M.; Kosugi, N.; Kuroda, H.; Kawamoto, A.; Tanaka, J.; Sugano, T.; Kinoshita, M.; Hino, S. *Synth. Met.* **1989**, *29*, F95-F102.

(13) Other structural types of higher coordination number have been prepared with M(pc) systems: (a) Wynne, K. J. *Inorg. Chem.* **1985**, *24*, 1339-1343. (b) Hanack, M. *Mol. Cryst. Liq. Cryst.* **1988**, *160*, 133-137. (c) Mossoyan-Deneux, M.; Benlian, D.; Baldy, A.; Pierrot, M. *Mol. Cryst. Liq. Cryst.* **1988**, *156*, 247-256. (d) Mossoyan-Deneux, M.; Benlian, D.; Pierrot, M.; Fournel, A.; Sorbier, J. P. *Inorg. Chem.* **1985**, *24*, 1878-1882. (e) Pietro, W. J.; Marks, T. J.; Ratner, M. A. *J. Am. Chem. Soc.* **1985**, *107*, 5387-5391.

0020-1669/91/1330-0803$02.50/0

Experimental Section

Preparation of Cu(tmp). Free-base 5,10,15,20-tetramethylporphyrin, H_2(tmp), was prepared by the condensation of pyrrole and acetaldehyde in glacial acetic acid. The synthesis of tmp uses nickel acetate as a template to produce Ni(tmp).[14] When the synthesis is performed under the same conditions but in the absence of a metal salt, only H_2(tmp) is formed. The yields for both of these syntheses are low (≈1%).

Metalation of H_2(tmp) (150 mg) with (acetylacetonato)copper(II) (300 mg) was performed in *N,N*-dimethylformamide (500 mL) at 60 °C. After 4 h the reaction mixture was cooled to room temperature and then placed in a freezer overnight. The impure Cu(tmp) was then filtered from the reaction solution and with the aid of an ultrasonic source was redissolved in $CHCl_3$. This solution was chromatographed through a silica column to afford optically pure Cu(tmp).

Preparation of [Cu(tmp)]$_2$[ReO$_4$]. Single crystals of [Cu(tmp)]$_2$[ReO$_4$] were grown at the anode of an electrolytic cell that consisted of two compartments separated by a frit of medium porosity. A 1,1,2-trichloroethane (TCE) solution 1.5×10^{-2} M in [N(*n*-Bu)$_4$][ReO$_4$] was saturated with Cu(tmp). This solution was filtered and placed in the electrolytic cell. Platinum electrodes were immersed in both compartments of the cell, and a constant current of 1 μA was passed through the cell for 1 week. Needle-shaped crystals of [Cu(tmp)]$_2$[ReO$_4$], rectangular in cross section, were harvested from the anode surface. Elemental analysis was carried out by Schwarzkopf Microanalytical Laboratory, Woodside, NY, and is consistent with the formula [Cu(tmp)]$_2$[ReO$_4$]. Anal. Calcd for $C_{48}H_{40}Cu_2N_8O_4Re$: C, 52.12; H, 3.65; N, 10.13. Found: C, 50.59; H, 3.64; N, 10.09.

X-ray Diffraction Study of [Cu(tmp)]$_2$[ReO$_4$]. Weissenberg photographs of [Cu(tmp)]$_2$[ReO$_4$] crystals are superimposable on those of [Ni(tmp)]$_2$[ReO$_4$].[5] From the photographs, these compounds were assigned to Laue group $4/m$ of the tetragonal system. The systematic absences ($hk0$, $h + k$ odd; $00l$, hhl, l odd) are consistent with space group C_{4h}^3–$P4/n$. The cell constants of the Cu salt were determined by a least-squares refinement of the setting angles of 16 reflections that had been hand-centered on a Picker FACS-I diffractometer. Intensity data were collected at 110 K with the θ–2θ scan technique.[15] No systematic changes were seen in the six standard reflections that were measured every 100 reflections. Experimental details and crystal data are summarized in Table I; more information is available in Table IS.[16]

After correction for absorption, the data equivalent in $4/m$ were averaged (R_{av} = 0.049). Initial refinement was on F_o, with the 2582 unique reflections having $F_o^2 > 3\sigma(F_o^2)$. All non-hydrogen atomic positions from the [Ni(tmp)]$_2$[ReO$_4$] structure were used as the starting values. Least-squares refinement on F_o with isotropic thermal parameters of all non-hydrogen atoms led to a value for R of 0.21; upon a change to anisotropic thermal parameters, the value decreased to 0.05. The hydrogen atom positions were determined from a difference electron density map, but in successive refinements their positions were idealized (C–H = 0.95 Å) and held constant. Each hydrogen atom was given an isotropic thermal parameter 1 Å^2 larger than that of the carbon atom to which it is bonded. The final refinement on F_o^2 converged to $R(F^2)$ = 0.069 for 4695 observations and 144 variables. The value of $\sum w(F_o^2 - F_c^2)^2$ as a function of $\lambda^{-1} \sin\theta$, F_o^2, and setting angles showed no unusual trends. A final difference electron density map shows no unexpected features. Except for a peak of 4.0 (2) e/Å^3 on the $\bar{4}$-fold axis 1 Å from Re, the highest density is 2.0 (2) e/Å^3, about 13% the height of a typical C atom in this structure. The final positional and equivalent isotropic thermal parameters are given in Table II. Table IIS[16] presents the anisotropic thermal parameters; Table IIIS[16] provides a listing of $10|F_o|$ vs $10|F_c|$.

Single-Crystal Electrical Conductivity Measurements. The single-crystal electrical conductivity of [Cu(tmp)]$_2$[ReO$_4$] was measured along the needle (c) axis with the use of a four-probe ac (27 Hz) phase-locked technique, as described elsewhere.[17] The sample dimensions ranged 0.1–0.3 mm in length and 3×10^{-3}–1×10^{-2} mm^2 in cross-sectional area. The uncertainties in the measurements of these dimensions lead to $\Delta(\sigma)/\sigma = \pm 0.2$. These needle-shaped crystals are too thin to enable the measurement of conductivity perpendicular to the needle axis.

Electron Spin Resonance Measurements. Powder and single-crystal ESR spectra were obtained on a modified Varian E-4 X-band (9.5 GHz) spectrometer or a Varian E-109 Q-band (35 GHz) spectrometer, both with 100-kHz field modulation, as described previously.[18]

Table II. Positional Parameters and Equivalent Isotropic Thermal Parameters for [Cu(tmp)]$_2$[ReO$_4$]

atom	x	y	z	B_{eq},[a] Å^2
Re	$^1/_4$	$^3/_4$	$^1/_2$	2.682 (8)
Cu(1)	$^1/_4$	$^1/_4$	0.37515 (14)	0.81 (1)
Cu(2)	$-^1/_4$	$-^1/_4$	0.12425 (15)	0.92 (1)
O	0.30286 (17)	−0.18471 (17)	0.35230 (66)	3.4 (1)
N(1)	0.14318 (14)	0.19689 (14)	0.37538 (49)	0.97 (5)
C(11)	0.12804 (17)	0.11524 (17)	0.37348 (58)	0.98 (5)
C(12)	0.04298 (17)	0.10205 (18)	0.37270 (63)	1.20 (6)
C(13)	0.00716 (17)	0.17441 (18)	0.37397 (62)	1.19 (6)
C(14)	0.07050 (16)	0.23287 (17)	0.37540 (59)	1.02 (5)
C(15)	0.18427 (17)	0.05536 (17)	0.37392 (60)	1.06 (6)
C(16)	0.15836 (18)	−0.03086 (17)	0.37264 (65)	1.35 (6)
N(2)	−0.17966 (15)	−0.15375 (15)	0.12565 (49)	1.06 (5)
C(21)	−0.20263 (19)	−0.07539 (17)	0.12540 (60)	1.15 (6)
C(22)	−0.13275 (20)	−0.02416 (18)	0.12655 (64)	1.42 (6)
C(23)	−0.06827 (20)	−0.07163 (20)	0.12371 (66)	1.55 (7)
C(24)	−0.09661 (18)	−0.15306 (19)	0.12490 (60)	1.20 (6)
C(25)	−0.04662 (18)	−0.21902 (18)	0.12537 (62)	1.19 (6)
C(26)	0.04234 (19)	−0.20563 (21)	0.12320 (70)	1.64 (7)
H1C(12)	0.017	0.052	0.372	2.2
H1C(13)	−0.048	0.185	0.374	2.2
H1C(22)	−0.133	0.033	0.128	2.4
H1C(23)	−0.014	−0.055	0.122	2.5
H1C(16)	0.102	−0.033	0.373	2.3
H2C(16)	0.178	−0.056	0.258	2.3
H3C(16)	0.178	−0.057	0.488	2.3
H1C(26)	0.068	−0.249	0.058	2.7
H2C(26)	0.054	−0.158	0.054	2.7
H3C(26)	0.062	−0.202	0.255	2.7

[a] $B_{eq} = (8\pi^2/3)\sum_i\sum_j U_{ij} a_i^* a_j^* \mathbf{a}_i \cdot \mathbf{a}_j$.

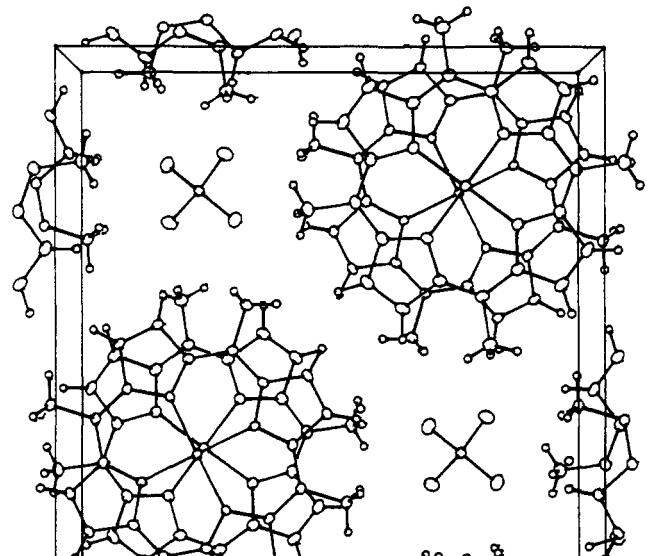

Figure 1. Structure of [Cu(tmp)]$_2$[ReO$_4$], as viewed along the [001] direction. Thermal ellipsoids are drawn at the 50% level except those for H atoms, which are drawn arbitrarily small.

Magnetic Susceptibility Measurements. The static magnetic susceptibility of [Cu(tmp)]$_2$[ReO$_4$] was measured with an SHE VTS-50 SQUID susceptometer. The sample holder was made of high-purity Spectrosil quartz (Thermal American, Inc.), and its background magnetic contribution was measured over the full temperature range just prior to examining the sample. The magnetism of [Cu(tmp)]$_2$[ReO$_4$] was determined at a field strength of 5 kG from the average of ten measurements made at each temperature. The raw data were corrected for temperature-independent magnetism ($\chi^{TI} = 1.2 \times 10^{-3}$ emu/mol) to afford the paramagnetic susceptibility χ^P. The sample weight was 8.5 mg.

(14) (a) Ulman, A.; Gallucci, J.; Fisher, D.; Ibers, J. A. *J. Am. Chem. Soc.* **1980**, *102*, 6852–6854. (b) Ulman, A.; Fisher, D.; Ibers, J. A. *J. Heterocycl. Chem.* **1982**, *19*, 409–413.
(15) Corfield, P. W. R.; Doedens, R. J.; Ibers, J. A. *Inorg. Chem.* **1967**, *6*, 197–204.
(16) Supplementary material.
(17) Phillips, T. E.; Anderson, J. R.; Schramm, C. J.; Hoffman, B. M. *Rev. Sci. Instrum.* **1979**, *50*, 263–265.
(18) Phillips, T. E.; Scaringe, R. P.; Hoffman, B. M.; Ibers, J. A. *J. Am. Chem. Soc.* **1980**, *102*, 3435–3444.

Table III. Distances (Å) and Angles (deg) for $[Cu(tmp)]_2[ReO_4]$[a]

bond	type	dist or angle	bond	type	dist or angle
Cu(1)–Cu(2)		3.369 (1)	C(11)–N(1)–C(14)	C_a–N–C_a	105.8 (2)
Cu(2)–Cu(1′)		3.377 (1)	C(21)–N(2)–C(24)		105.9 (2)
av		3.373 (6)	av		105.8 (2)
Cu(1)–N(1)	M–N	2.001 (2)	N(1)–C(11)–C(12)	N–C_a–C_b	109.3 (2)
Cu(2)–N(2)		2.000 (3)	N(1)–C(14)–C(13)		111.0 (2)
av		2.000 (3)	N(2)–C(21)–C(22)		109.9 (3)
N(1)–C(11)	N–C_a	1.393 (4)	N(2)–C(24)–C(23)		109.7 (3)
N(1)–C(14)		1.361 (4)	av		110.0 (7)
N(2)–C(21)		1.370 (4)	N(1)–C(11)–C(15)	N–C_a–C_m	126.3 (3)
N(2)–C(24)		1.393 (4)	N(1)–C(14)–C(15)		126.7 (3)
av		1.379 (17)	N(2)–C(21)–C(25)		126.5 (3)
C(11)–C(12)	C_a–C_b	1.444 (4)	N(2)–C(24)–C(25)		126.7 (3)
C(13)–C(14)		1.446 (4)	av		126.5 (3)
C(21)–C(22)		1.454 (4)	C(11)–C(12)–C(13)	C_a–C_b–C_b	107.5 (3)
C(23)–C(24)		1.446 (4)	C(12)–C(13)–C(14)		106.4 (2)
av		1.448 (4)	C(21)–C(22)–C(23)		107.4 (3)
C(12)–C(13)	C_b–C_b	1.354 (4)	C(22)–C(23)–C(24)		107.2 (3)
C(22)–C(23)		1.343 (5)	av		107.1 (5)
av		1.349 (8)	C(12)–C(11)–C(15)	C_b–C_a–C_m	124.4 (3)
C(11)–C(15)	C_a–C_m	1.378 (4)	C(13)–C(14)–C(15)		122.4 (3)
C(14)–C(15)		1.413 (4)	C(22)–C(21)–C(25)		123.6 (3)
C(21)–C(25)		1.400 (4)	C(23)–C(24)–C(25)		123.6 (3)
C(24)–C(25)		1.388 (4)	av		123.5 (8)
av		1.395 (15)	C(11)–C(15)–C(14)	C_a–C_m–C_a	122.8 (3)
C(15)–C(16)	C_m–C_t	1.510 (4)	C(21)–C(25)–C(24)		122.7 (3)
C(25)–C(26)		1.510 (4)	av		122.8 (3)
av		1.510 (4)	C(11)–C(15)–C(16)	C_a–C_m–C_t	120.1 (3)
N(1)–Cu(1)–N(1)	N–M–N′	90	C(14)–C(15)–C(16)		117.1 (3)
N(2)–Cu(2)–N(2)		90	C(21)–C(25)–C(26)		118.7 (3)
av		90	C(24)–C(25)–C(26)		118.6 (3)
Cu(1)–N(1)–C(11)	M–N–C_a	126.9 (2)	av		118.6 (12)
Cu(1)–N(1)–C(14)		127.2 (2)	Re–O		1.726 (3)
Cu(2)–N(2)–C(21)		127.5 (2)	O–Re–O		109.5 (3)
Cu(2)–N(2)–C(24)		126.6 (2)			
av		127.1 (4)			

[a] Rotation angle between intrastack Cu(tmp) molecules: 27.4 (1)°. The notation is that of: Hoard, J. L. *Science (Washington D.C.)* **1971**, *174*, 1295–1302. C_t is the methyl group on the methine carbon. The number in parentheses is the larger of the standard deviation of a single observation as estimated from the inverse matrix or from the values averaged.

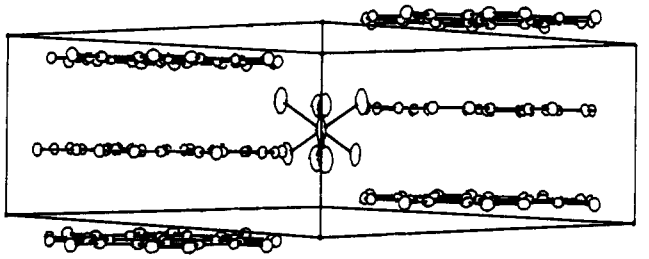

Figure 2. Structure of $[Cu(tmp)]_2[ReO_4]$, as viewed along the [110] direction.

Results and Discussion

Description of the Structure. $[Cu(tmp)]_2[ReO_4]$ is isostructural with $[Ni(tmp)]_2[ReO_4]$,[5] with the Cu(tmp) cations arranged in columns surrounded by anions. Figure 1 shows the stacking of Cu(tmp) groups as viewed along the [001] direction. These molecules, which have crystallographically imposed 4 symmetry, stack metal-over-metal with their mean planes orthogonal to the *c* axis. The ReO_4 anion lies within the channels formed by the Cu(tmp) columns on a site of crystallographically imposed $\bar{4}$ symmetry. There is no evidence for disorder of the anion. The arrangement of the anions and columns of macrocycles is shown in Figure 2.

The crystal structure of $[Cu(tmp)]_2[ReO_4]$ contains two independent Cu(tmp) cations that are rotated by 27.4 (1)° about the *c* axis with respect to one another. This angle is not significantly different from that observed in $[Ni(tmp)]_2[ReO_4]$ (27.5 (1)°). A drawing of Cu(tmp) cation 1 with the labeling scheme

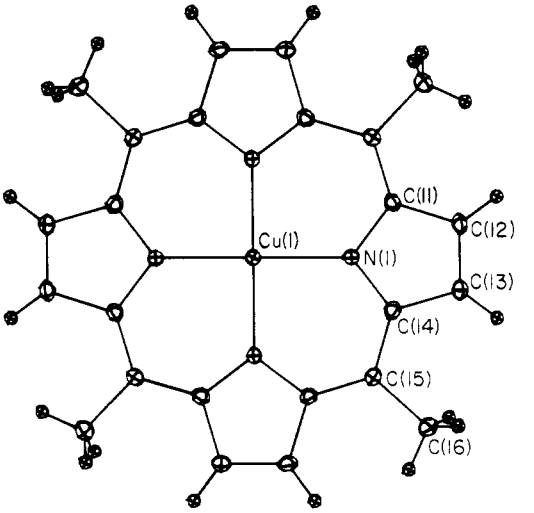

Figure 3. Drawing of one Cu(tmp) molecule with labeling scheme.

is shown in Figure 3. Table III summarizes the intramolecular bond distances and angles for $[Cu(tmp)]_2[ReO_4]$. The Cu(tmp) cations (symmetry 4) are planar (maximum deviation 0.008 Å), although planarity is not crystallographically imposed. The best weighted least-squares planes are given in Table IVS.[16]

The Cu–Cu spacings along the stacking axis alternate, with the Cu(1)–Cu(2) and Cu(2)–Cu(1′) distances being 3.369 (1) and 3.377 (1) Å, respectively. These distances are slightly larger than those observed for $[Ni(tmp)]_2[ReO_4]$, Ni(1)–Ni(2) = 3.355 (2)

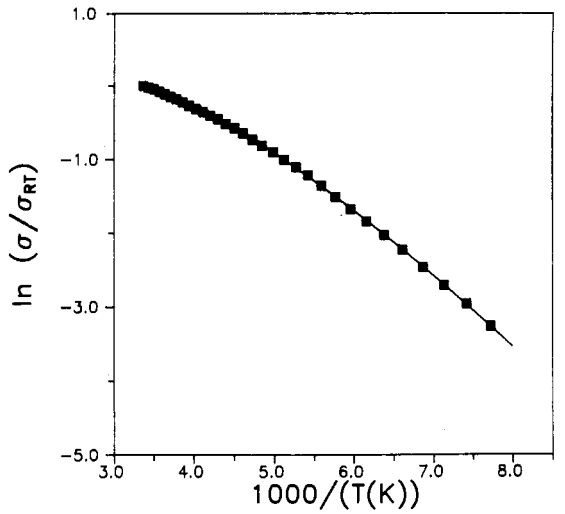

Figure 4. Conductivity along the needle *c* axis of $[Cu(tmp)]_2[ReO_4]$ as a function of temperature.

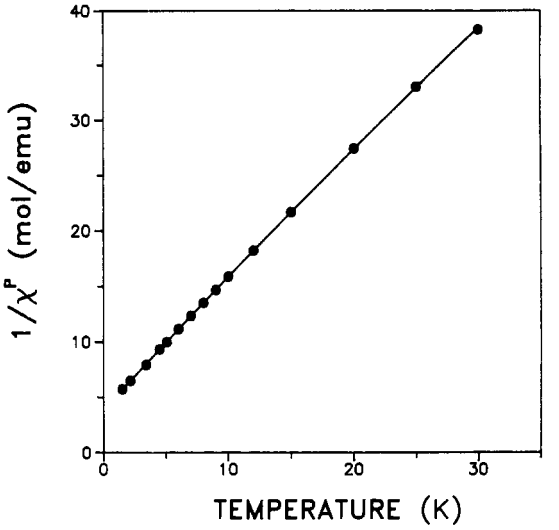

Figure 5. Temperature dependence of the paramagnetic susceptibility.

Å and Ni(2)–Ni(1′) = 3.365(2) Å, but are still within the van der Waals contact distance for carbon (3.4 Å).[19] Similarly, the M–N bonds in $[Cu(tmp)]_2[ReO_4]$ are slightly longer than those in $[Ni(tmp)]_2[ReO_4]$. The difference between the average Cu–N distance (2.000 (3) Å) and Ni–N distance (1.959 (4) Å) is 0.041 (5) Å.[20]

Single-Crystal Electrical Conductivity. Crystals of $[Cu(tmp)]_2[ReO_4]$ have a room-temperature conductivity in the range σ_{RT} = 30–50 Ω^{-1} cm^{-1}. These values are roughly half those observed for $[Ni(tmp)]_2[ReO_4]$.[5] The best crystals of the other Ni(tmp)-based conductors synthesized to date display higher conductivity, with room-temperature values as high as 270 Ω^{-1} cm^{-1} for Ni(tmp)I[6] and 200 Ω^{-1} cm^{-1} for $[Ni(tmp)]_2[PF_6]$.[6] These values may also be compared to those of the related phthalocyanine salts Ni(pc)I[1] (σ_{RT} = 500 Ω^{-1} cm^{-1}) and Cu(pc)I[2] (σ_{RT} = 10^3 Ω^{-1} cm^{-1}).

The conductivity of $[Cu(tmp)]_2[ReO_4]$ is thermally activated, decreasing as the temperature is reduced (Figure 4). These data obey an expression that describes a semiconductor with a thermally activated carrier mobility:[21]

$$\sigma/\sigma_0 = T^{-\alpha} \exp(-\Delta E/k_B T) \qquad (1)$$

where σ/σ_0 is the normalized conductivity, α is a mobility parameter, ΔE is the activation energy for conduction, and k_B is Boltzmann's constant. A least-squares fit of the data to eq 1 yields α = 3.8 (2) and ΔE = 0.126 (2) eV. This value for ΔE is about half that for the more conductive $[Ni(tmp)]_2[ReO_4]$ system (ΔE = 0.24 (2) eV).[5] The difference between the conductivities of $[Ni(tmp)]_2[ReO_4]$ and $[Cu(tmp)]_2[ReO_4]$ may arise from the slightly larger interplanar distances observed in the Cu salt or from paramagnetic scattering of the carrier electrons by the Cu(II) ions.

Magnetism. The magnetism of $[Cu(tmp)]_2[ReO_4]$ arises from two spin systems, the spins localized on Cu(II) (d^9, $S = {}^1/_2$) metal sites and the ligand-based itinerant charge carriers. As we will show, these two spin systems are exchange-coupled. In addition, intrachain Cu–Cu spin exchange results from direct Cu–Cu interactions as well as indirect coupling mediated by electrons in the partially oxidized π orbitals of the macrocycle.

The paramagnetic susceptibility (χ^P = 2.6 (1) × 10^{-2} emu/mol) of $[Cu(tmp)]_2[ReO_4]$ arises from the two separate spin systems. The susceptibility of the Cu(II) sites, χ^{Cu}, is expected to follow the Curie–Weiss law; that of the carrier electrons, χ^{π}, is expected to follow a simple Curie law, but the number of carriers in this semiconductor is expected to increase exponentially with temperature. The total paramagnetic susceptibility is the sum of these two components, and its temperature dependence is given by

$$\chi^P(T) = \chi^{Cu}(T) + \chi^{\pi}(T)$$
$$= C/(T - \Theta) + nT^{-1} \exp(-\Delta E_\chi/k_B T) \qquad (2)$$

where C and Θ are respectively the Curie and Weiss constants for the Cu(II) spin system and ΔE_χ is an activation energy for π-carrier formation. However, since the number of carriers is small compared with the number of Cu spins, their influence on the bulk susceptibility is negligible, $n \ll C$. Therefore, the susceptibility data yield useful information only on the copper spin system.

The temperature dependence of $1/\chi^P$ is shown in Figure 5. The data have been fit to the Curie–Weiss equation to give C = 0.804 (8) emu K mol^{-1} and Θ = −3.1 (1) K. The value of the Curie constant is in excellent agreement with that of 0.813 emu K mol^{-1} calculated for two Cu spins per formula unit from the equation

$$C = S(S + 1)(2Ng^2\beta^2/3k_B) \qquad (3)$$

where N is the number of Cu(II) sites per mole, β is the Bohr magneton, $S = {}^1/_2$, and $g^2 = (2g_\perp{}^2 + g_\parallel{}^2)/3 = 4.334$ is the average square of the spectroscopic splitting factor. Since the full susceptibility of the Cu spins is observed, all the Cu sites must retain the $S = {}^1/_2$ d^9 oxidation state, with no oxidation occurring at the metal. The Weiss constant (Θ = −3.1 (1) K) is indicative of antiferromagnetic Cu–Cu coupling within the chains; its value is comparable to those observed in other Cu macrocyclic conductors, for example Cu(pc)I (Θ = −4.18 (3) K),[2] Cu(tatbp)I (Θ = −6.9 (3) K),[3] and $[Cu(tatbp)]_3[ReO_4]_2{\cdot}C_{10}H_7Cl$ (Θ = −5.2 (3) K).[4]

In the absence of exchange interactions between the local Cu(II) moments and the itinerant π-carriers, the ESR signal of $[Cu(tmp)]_2[ReO_4]$ would exhibit two separate resonances. The signal arising from the Cu(II) sites would have a **g** tensor similar to that found for Cu(tmp) diluted into Ni(tmp) ($g_\parallel$ = 2.20 and $g_\perp$ = 2.02). The π-carriers would have an isotropic **g** tensor similar to that observed for $[Ni(tmp)]_2[ReO_4]$ (g = 2.00).[5] Instead, strong exchange coupling ($J \gg (g_{Cu} - g_\pi)\beta H_0$) between local and itinerant spin systems produces a single signal with temperature-dependent g values. At all temperatures, the **g** tensor of $[Cu(tmp)]_2[ReO_4]$ is axially symmetric, as expected from the site symmetry at Cu. The angular dependence of the g value at room temperature (Figure 6) may be described by

$$g(\Phi) = [g_\parallel{}^2 \cos^2 \Phi + g_\perp{}^2 \sin^2 \Phi]^{1/2} \qquad (4)$$

where Φ is the angle between the unique tensor axis (crystallo-

(19) Bondi, A. *J. Phys. Chem.* **1964**, *68*, 441–451.

(20) The only other possibly significant differences between the Ni and Cu structures are

	Ni	Cu
C(14)–C(15), Å	1.392 (6)	1.413 (4)
C(21)–N(2)–C(24), deg	104.5 (4)	105.9 (2)
N(2)–C(21)–C(22), deg	111.1 (4)	109.9 (3)

(21) (a) Kittel, C. *Introduction to Solid State Physics*; Wiley: New York, 1976. (b) Epstein, A. J.; Conwell, E. M.; Sandman, D. J.; Miller, J. S. *Solid State Commun.* **1977**, *23*, 355–358.

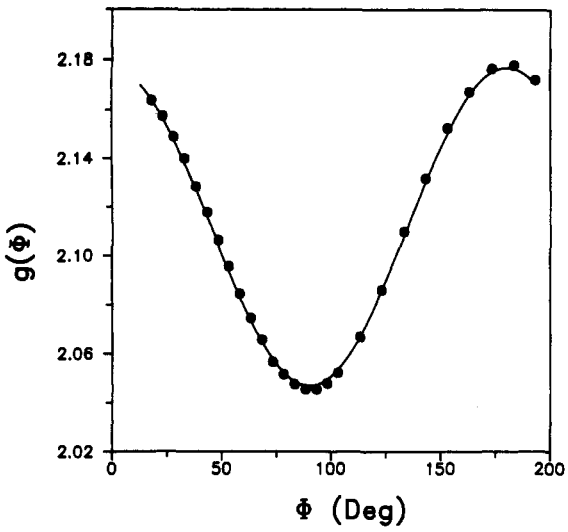

Figure 6. Dependence of the ESR g value on Φ, the angle between the crystallographic c axis and the applied magnetic field (room temperature).

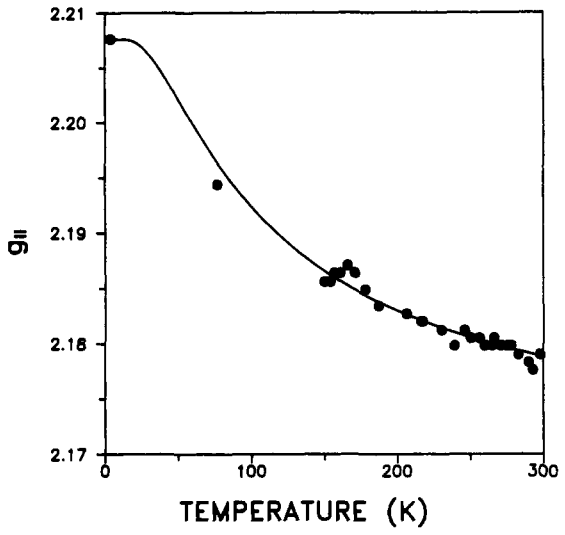

Figure 7. Temperature dependence of $g_\parallel$ ($\Phi = 0°$) for a single crystal of $[Cu(tmp)]_2[ReO_4]$. The solid line represents the best fit to eq 5.

graphic c) and the applied magnetic field. A least-squares fit of these data yields the values $g_\parallel(RT) = 2.177$ (1) and $g_\perp(RT) = 2.047$ (1). These values are intermediate between those expected for isolated Cu(tmp) molecules and π-carriers. This is expected since the g values of an exchange-coupled system occur at the susceptibility-weighted average of the g values for the individual components (eq 5a).[2] In the present case $g^{Cu}(\Phi)$ is the angle-

$$g_{obs}(\Phi,T) = g^{Cu}(\Phi) f^{Cu}(T) + g^{\pi}(1 - f^{Cu}(T)) \quad (5a)$$

$$g^{Cu}(\Phi) = [(g_\parallel{}^{Cu})^2 \cos^2 \Phi + (g_\perp{}^{Cu})^2 \sin^2 \Phi]^{1/2} \quad (5b)$$

$$f^{Cu}(T) = \chi^{Cu}(T)/(\chi^{Cu}(T) + \chi^{\pi}(T)) \quad (5c)$$

dependent g value of the one-dimensional chains of Cu(II) spins (eq 5b) and g^π is the isotropic g value of the π-carriers. The parameters $g_\parallel{}^{Cu}$ (2.208 (1)) and $g_\perp{}^{Cu}$ (2.045 (1)) were derived from measurements on single crystals of $[Cu(tmp)]_2[ReO_4]$ at 4.2 K.[22] The free-electron value ($g_\parallel$ of 2.002) was used for the ligand-based π-carriers. The fraction $f^{Cu}(T)$ of the total susceptibility arising from the Cu spins is given by eq 5c, where

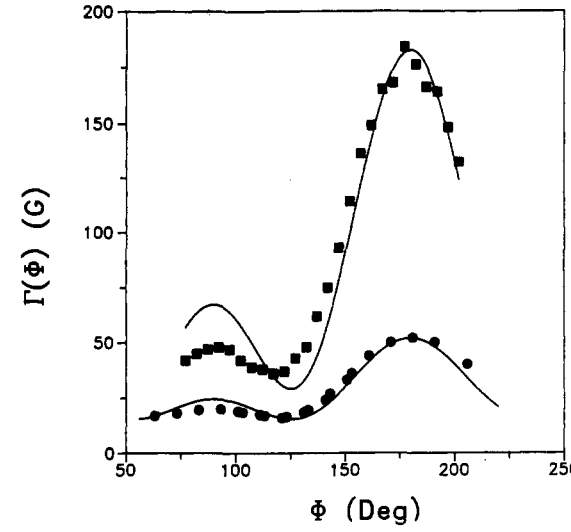

Figure 8. ESR line width as a function of Φ at room temperature (circles) and 4.2 K (squares).

$\chi^{Cu}(T)$ and $\chi^{\pi}(T)$ are the temperature-dependent susceptibilities of the Cu spin system and the π-carriers, respectively (eq 2).[2] When the experimental temperature dependence of $g_\parallel$ was fit to eqs 5 and 2, by using the value of C derived from the static susceptibility measurement, values of n of 0.19 emu K mol^{-1} and ΔE_χ of 9.2×10^{-3} eV were obtained (Figure 7). This activation energy (ΔE_χ) is much smaller than that observed for conduction ($\Delta E_\sigma = 0.12$ eV). It is likely that these values differ because the carrier mobility is thermally activated and the activation energy for conduction is composed of an energy for carrier formation ΔE_χ and an energy associated with a carrier-hopping mechanism ΔE_{hop}, namely, $\Delta E_\sigma = \Delta E_\chi + \Delta E_{hop}$.

Further evidence that χ_π arises from the mobile carrier electrons and not from localized paramagnetic sites with $g = 2.00$ is afforded by the ESR line widths. If the Cu(II) spin system were coupled to localized π-cation radicals, the number of such radicals would not be large enough for each Cu(II) site to possess an identical environment since some Cu(II) sites would be closer to the π-cation radicals than others. The resultant range of Cu–π couplings would produce a range of observed g values, and a large portion of the ESR line width would result from this inhomogeneity in the g value and would be frequency dependent. But the line widths are identical at X-band (9.5 GHz) and Q-band (35 GHz) frequencies, and thus all the Cu sites must be equally coupled to the $g = 2.00$ spin system. The simplest explanation for this type of homogeneous coupling is that the spins in the $g = 2.00$ system are mobile charge carriers, and the delocalization of this small number of spins averages the environments of the Cu sites.

Single crystals of $[Cu(tmp)]_2[ReO_4]$ exhibit an axial line-width tensor. The room-temperature line width at $g_\parallel$ is 50 (2) G and at $g_\perp$ is 21 (1) G. The angular dependence of the line width can be fit to the functional form

$$\Gamma(\Phi) = \Gamma_1(3 \cos^2 \Phi - 1)^2 + \Gamma_0 \quad (6)$$

with a dipolar component $\Gamma_1 = 7.6$ (5) G and an isotropic component $\Gamma_0 = 17.4$ (5) G at room temperature (Figure 8). The functional form of eq 6 can arise in two cases.[4b] First, it will occur in the weak-exchange limit, where the exchange frequency $\omega_e = J/h$ for coupling between adjacent dipoles is considerably smaller than the Larmor frequency, $\omega_e \ll \omega_0$, or second, it will occur if the exchange is strongly one-dimensional.

Weak exchange can be ruled out for $[Cu(tmp)]_2[ReO_4]$, for this would require the bulk susceptibility to exhibit a Weiss constant $|\Theta| < \hbar\omega_0/k_B \approx 0.5$ K, much smaller than the observed value of 3.1 K. Moreover, if one assumes $\omega_e \ll \omega_0$ and calculates ω_e using standard equations[2a] that express the dipolar line width $\Gamma_1 = 7.6$ G in terms of the average Cu–Cu distance, then one arrives at an internal inconsistency because the calculation gives $\omega_e = 2.5 \times 10^{12}$ s$^{-1} \gg \omega_0$(X-band) $= 6 \times 10^{10}$ s^{-1}. Instead, the second case must apply, and the angular dependence of Γ may

(22) The g values at 4.2 K were used in the model because χ_π is negligible at this temperature. The g values for isolated, unoxidized molecules of Cu(tmp) may not reflect the limiting values for the molecules in this compound because the porphyrins are not planar in the unoxidized phase; see ref 23.

(23) Gallucci, J. C.; Swepston, P. N.; Ibers, J. A. *Acta Crystallogr.* **1982**, *B38*, 2134–2139.

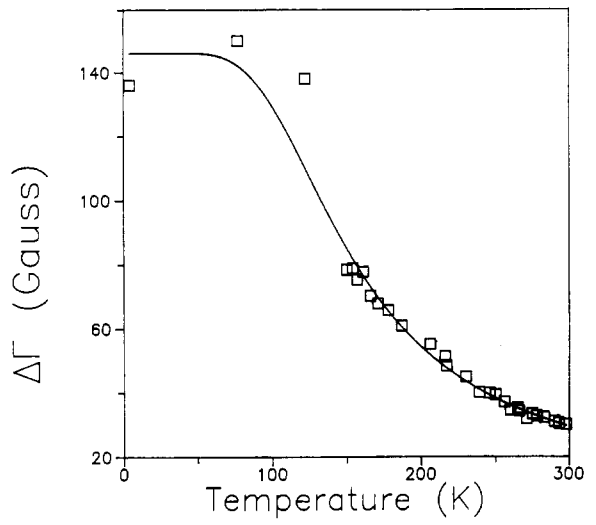

Figure 9. Plot of $\Delta\Gamma$ as a function of temperature.

be accounted for by assuming strong Cu–Cu coupling along the chain only, J(intrachain) $\gg$ J(interchain), consistent with the crystal structure in which Cu chains are separated by 16.774 (9) Å.

As the crystals are cooled from room temperature, the line width increases exponentially until 100 K. Below 100 K, the line width is nearly constant with changing temperature. Figure 9 illustrates the temperature dependence of the dipolar line width $\Delta\Gamma = \Gamma_{\parallel} - \Gamma_{\perp}$. Since the angular dependence of the line width is dominated by the Cu dipolar interaction, the parallel and dipolar line widths exhibit the same temperature dependence. We may ascribe the temperature dependence of the dipolar line width to exchange narrowing of the dipolar interaction along the one-dimensional chain of Cu atoms, where the exchange frequency is temperature dependent: $\hbar\omega_e = k_B[A + B\exp(-\Delta E_\Gamma/k_BT)]$. The constant A, the temperature-independent component of the exchange, is attributed to the direct interaction of the Cu spins; the temperature-dependent component (B) is attributed to indirect exchange mediated by the carrier spins. Insertion of this expression for the exchange interaction into the functional form for the dipolar line width in the strong-exchange limit yields the expression

$$\Delta\Gamma(T) = \frac{8}{3\sqrt{3}} \frac{m_D}{k_B[A + B\exp(-\Delta E_\Gamma/k_BT)]} \qquad (7)$$

The value for the second moment for the Cu(II) chains, m_D/k_B = 92 G K, was calculated from standard formulas and the average Cu–Cu spacing of 3.373 (6) Å.[3a,24] A fit of the line width data between 4.2 and 298 K to eq 7 yields an activation energy of ΔE_Γ = 0.044 (1) eV, A = 0.98 K, and B = 2.15 K. The exponential increase of the exchange narrowing with temperature and the relative sizes of A and B are evidence that the carrier electrons play a significant role in mediating indirect Cu–Cu spin exchange above 100 K. To this extent, the present results are consistent with those for the metallic conductors Cu_xNi_{1-x}(pc)I.[25] The interpretation of the magnitude of the activation parameter ΔE_Γ, like that of ΔE_χ, again may be complicated by details of the thermally activated carrier mobility.

Conclusions

$[Cu(tmp)]_2[ReO_4]$ is a ligand-oxidized material whose conduction band is formed from porphyrin p–π orbitals. The structures and conductivities of $[Ni(tmp)]_2[ReO_4]$ and $[Cu(tmp)]_2[ReO_4]$ are nearly identical, but their magnetic properties are very different. In $[Ni(tmp)]_2[ReO_4]$ the magnetic behavior results solely from the π-carrier electrons. The Cu salt contains two separate spin systems, the localized Cu(II) moments and the mobile π-carriers. When the magnetic properties of the present compound are compared to similar conductors, it is clear that Cu–Cu magnetic interactions in this semiconducting material are governed by carrier concentration and mobility, as they are in metallic conductors.

The spin systems of Cu(pc)I and $[Cu(tmp)]_2[ReO_4]$ are similar in that both have localized magnetic moments centered on the Cu(II) ions embedded within the conductive framework of the macrocycle. However, Cu(pc)I[2] is a molecular metal. In this phase strong intramolecular spin exchange between the metallic carriers in the partially ($+^1/_3$) oxidized ligand and the local Cu(II) moments leads to long-range carrier-mediated Cu–Cu coupling. The Weiss constant of −4.18 (3) K and the ESR line width angular dependence ($\Gamma \propto (\cos^2\Phi + 1)$) support this description. The **g** tensor of Cu(pc)I, which is the susceptibility-weighted average of the Cu and π systems, exhibits linear rather than exponential temperature dependence because no activation parameter is involved. The number of π-carriers does not change with temperature as it does in $[Cu(tmp)]_2[ReO_4]$.

In $[Cu(tmp)]_2[ReO_4]$ the conductivity is significant but thermally activated. The Weiss constant of −3.1 (1) K is comparable to that of Cu(pc)I, indicating strong Cu–Cu exchange. Unlike the case of Cu(pc)I, however, the activated nature of the charge carriers in $[Cu(tmp)]_2[ReO_4]$ results in an exponential temperature dependence of the g value. The ESR measurements show that strong Cu–π spin exchange occurs in this phase but the Cu–Cu coupling mediated by this interaction depends on the concentration and mobility of the carriers and decreases as temperature is lowered. The limited mobility of the carrier electrons may also explain the different forms of the angular dependence of the ESR line width in $[Cu(tmp)]_2[ReO_4]$ and Cu(pc)I. The $3\cos^2\Phi - 1$ dependence reported here is interpreted as implying strictly one-dimensional exchange. The more mobile electrons of Cu(pc)I are more likely to move between the chains of cations than those of $[Cu(tmp)]_2[ReO_4]$, and so $[Cu(tmp)]_2[ReO_4]$ is more likely to fulfill this criterion.

Acknowledgment. This work was supported by the National Science Foundation through Grant DMR-8818599 (B.M.H.) and through the Northwestern University Materials Research Center, Grant DMR-8821571 (B.M.H. and J.A.I.).

Registry No. H_2(tmp), 54976-00-0; TCE, 79-00-5; Cu(tmp), 63022-59-3; $[Cu(tmp)]_2[ReO_4]$, 131435-31-9; $[N(n\text{-}Bu)_4][ReO_4]$, 16385-59-4; Pt, 7440-06-4; (acetylacetonato)copper(II), 13395-16-9.

Supplementary Material Available: Complete crystallographic details (Table IS), anisotropic thermal parameters (Table IIS), and best weighted least-squares planes (Table IVS) (4 pages); $10|F_o|$ vs $10|F_c|$ (Table IIIS) (20 pages). Ordering information is given on any current masthead page.

(24) McGregor, K. T.; Soos, Z. G. *J. Chem. Phys.* **1976**, *64*, 2506–2517.
(25) Ogawa, M. Y.; Palmer, S. M.; Liou, K. K.; Quirion, G.; Thompson, J. A.; Poirier, M.; Hoffman, B. M. *Phys. Rev. B* **1989**, *39*, 10682–10692.